Computed Encapsulation Energetics for Metallofullerenes

Zdeněk Slanina,*,** Filip Uhlík*** and Shigeru Nagase**

**Department of Theoretical and Computational Molecular Science, Institute for Molecular Science, Myodaiji, Okazaki 444-8585, Aichi, Japan
***School of Science, Charles University, 128 43 Prague 2, Czech Republic

Abstract: Some alkali and alkaline-earth metals can be now encapsulated in fullerenes. For example, $Li@C_{60}$ and $Li@C_{70}$ can be produced by the low-energy bombardment method while $Ca@C_{74}$, $Sr@C_{74}$, and $Ba@C_{74}$ can be prepared by high-temperature syntheses. Hence, their computations at higher levels of theory are also of interest. In the report, the computations are carried out on $Li@C_{60}$, $Li_2@C_{60}$ and $Li_3@C_{60}$ with the B3LYP and MPWB1K density-functional theory (DFT) treatment in the standard 3-21G and 6-31G* basis sets. The computed energetics suggests that $Li_x@C_{60}$ species could be produced for several small x values if the Li pressure is enhanced sufficiently. The B3LYP DFT approach is also applied to $Mg@C_{74}$, $Ca@C_{74}$, $Sr@C_{74}$, and $Ba@C_{74}$ and production populations are thus rationalized.

Keywords: Endohedral fullerenes; carbon-based nanotechnology; molecular modeling; molecular electronic structure; metallofullerene stabilities.

INTRODUCTION

There has been a renewed interest [1-22] in systems containing alkali metals and fullerenes, in particular $Li@C_{60}$ and $Li@C_{70}$ produced by low energy ion implantation [11,13,14] in bulk amounts. Recently, such systems have also been subjected to more advanced computations [19-22], especially in the studies by Gurin [19,20]. The vibrational spectra were obtained [13,14] for $Li@C_{60}$ and $Li@C_{70}$. $Li_2@C_{60}$ was also evidenced in observations [11] though in a small amount compared to $Li@C_{60}$. In addition to alkali metals, even alkaline-earth metals can be encapsulated into fullerene cages and actually a whole reaction series $Ca@C_{74}$, $Sr@C_{74}$, and $Ba@C_{74}$ is now available from high-temperature techniques [23-25]. The observations moreover suggest a qualitative information on their relative populations. The recent experimental progress makes computations of the species even more interesting and, in particular, some theoretical rationalization of the observed relative stabilities would be useful. In the report, the computations are carried out on $Li@C_{60}$, $Li_2@C_{60}$, and $Li_3@C_{60}$, and also on $Mg@C_{74}$, $Ca@C_{74}$, $Sr@C_{74}$, and $Ba@C_{74}$, using the density-functional theory (DFT) treatments. The report supplies illustrative examples what kind of information can be obtained from calculations for such metallofullerene systems. Both potential energy and Gibbs free energy terms are evaluated. The study for the first time allows for computational rationalization of the observed relative populations for metallofullerene reaction series.

COMPUTATIONS

The geometry optimizations were carried out with Becke's three parameter functional [27] with the non-local Lee-Yang-Parr correlation functional [28] (B3LYP) in the standard 3-21G basis set (B3LYP/3-21G). The geometry optimizations were carried out with the analytically constructed energy gradient as implemented in the Gaussian program package [29]. Although the 3-21G basis set is a small basis, its application has been customary for fullerene geometries owing to the computational demands (though a check with larger basis sets would in future be useful).

In the optimized B3LYP/3-21G geometries, the harmonic vibrational analysis was carried out with the analytical force-constant matrix. In the same optimized geometries, higher-level single-point energy calculations were also performed, using the standard 6-31G* basis set, i.e., the B3LYP/6-31G* level (or, more precisely, B3LYP/6-31G*//B3LYP/3-21G). As $Li@C_{60}$ and $Li_3@C_{60}$ are radicals, their computations were carried out using the unrestricted B3LYP treatment for open shell systems (UB3LYP). The ultrafine integration grid was used for the DFT numerical integrations throughout.

Recently, Zhao and Truhlar [30-35] performed a series of test DFT calculations with a conclusion [35] that the MPWB1K functional (the modified Perdew and Wang exchange functional MPW [36] and Becke's meta correlation functional [37] optimized against a kinetics database) is the best combination for evaluations of nonbonded interactions with a relative averaged mean unsigned error of only 11%. The MPWB1K functional is also applied in this report.

RESULTS AND DISCUSSION

One atom-type stepwise encapsulations: $Li_x@C_{60}$

The UB3LYP approach is preferred here over the restricted open-shell treatment (ROB3LYP) as the latter actually

---
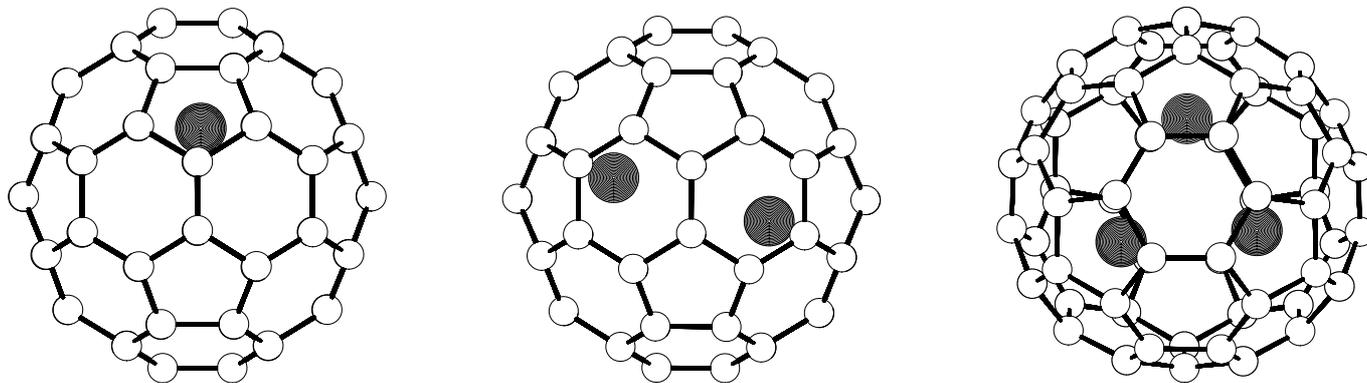
Fig. 1. B3LYP/3-21G optimized structures of $Li_x@C_{60}$ (the Li atoms are darkened).

exhibits a slow SCF convergency for the present systems (and ROB3LYP analytical frequencies are not implemented in the Gaussian program package [29]). Although the unrestricted Hartree-Fock (UHF) approach can be faster, it can also be influenced by the so called spin contamination [38] and indeed, this factor was an issue in our previous [15] UHF SCF calculations as the UHF/3-21G spin contamination turned out to be higher than recommended threshold [38] in the expectation value for the $< S^2 >$ term where S stands for the total spin. As long as the deviations from the theoretical value are smaller than 10%, the unrestricted results have traditionally been considered [38] applicable. This requirement is well satisfied for the $Li@C_{60}$ and $Li_3@C_{60}$ species - for example, at the B3LYP/3-21G level the expectation value is 0.7552 and 0.7546 for $Li@C_{60}$ and $Li_3@C_{60}$, respectively, i.e., closer less than 1% to the theoretical value. Fig. 1 shows the computed structures of $Li@C_{60}$, $Li_2@C_{60}$, and $Li_3@C_{60}$. In all the three cases the Li atoms in the optimized structures are shifted from the cage center towards its wall. In particular, in the $Li@C_{60}$ species the shortest computed Li-C distance is 2.26 Å while in a central location (which is a saddle point) the shortest Li-C distance at the UB3LYP/3-21G level is 3.49 Å. As for the energetics of the centric and off-centric location, the saddle point is placed by some 9.9 kcal/mol higher at the UB3LYP/3-21G level. However, the energy separation is further increased in the UB3LYP/6-31G*//UB3LYP/3-21G treatment, namely to 15.0 kcal/mol.

In the $Li_2@C_{60}$ case, the shortest Li-C distance is even bit shorter, 2.14 Å. On the other hand, the Li-Li separation is computed as 3.29 Å, i.e., substantially longer than the observed value in the free Li_2 molecule (2.67 Å, cf. refs. [39-41]). In the third species, $Li_3@C_{60}$, the shortest computed Li-C contact is even further reduced to 2.05 Å. The Li-Li distances in the encapsulated Li_3 cluster are not equal - they are computed as 2.70, 2.76 and 2.84 Å. Incidentally, while the observed Li-Li distance for free Li_2 is [39-41] 2.67 Å, the B3LYP/3-21G computed value is 2.725 Å (it changes to 2.723 Å at the B3LYP/6-31G* level). Similarly, also the observed values for the free Li_3 cluster are available [42,43], actually for two triangular forms - opened (2.73, 2.73, 3.21 Å) and closed (3.05, 3.05, 2.58 Å). The UB3LYP/3-21G computed distances in the free Li_3 opened cluster are 2.78, 2.78, and 3.30 Å. Hence, there is a good theory-experiment agreement. The formal Mulliken charge (the largest value) found on the Li atoms is somewhat decreasing in the $Li@C_{60}$, $Li_2@C_{60}$, and $Li_3@C_{60}$ series with the UB3LYP/3-21G values of 1.16, 1.10, and 0.86, respectively. Still, the total charge transferred to the cage is increasing in the series: 1.16, 2.21, and 2.46 (the charges are reduced in the 6-31G* basis).

The vibrational analysis enables to test if a true local energy minimum was found. All the computed frequencies for the structures in Fig. 1 are indeed real and none imaginary (though we could also locate some saddle points not discussed here). Moreover, the vibrational frequencies are primarily used here (together with other computed molecular parameters) for the entropy and thus Gibbs free-energy evaluations. Hence, the spectroscopic aspects are not of particular interest in our connections, however, let us mention relationships to some observed values. The lowest computed vibrational frequencies are mostly represented by motions of the Li atoms. Obviously, owing to symmetry reductions upon encapsulation, the symmetry selection rules do not operate any more in the way they simplify the C_{60} vibrational spectra [44]. Hence, the vibrational spectra of $Li_x@C_{60}$ must be considerably more complex than for the icosahedral (empty) C_{60} cage with just four bands in its IR spectrum [44]. This increased spectral complexity has indeed been observed [13,14]. Incidentally, the observed harmonic frequency [39-41] for free Li_2 is 351 cm^{-1} while the computed B3LYP/3-21G term is 349 cm^{-1} (and the B3LYP/6-31G* value 342 cm^{-1}). For the endohedrals, a larger-basis frequency calculations are not yet common, at least not throuhout a larger reaction series, though a check at a more advanced level would be interesting.

Different atom-type encapsulations: $X@C_{74}$

There is a general stability problem related to fullerenes and metallofullerenes - either the absolute stability of the species or the relative stabilities of clusters with different stoichiometries. One can consider an overall stoichiometry of a metallofullerene formation:

$$xY(g) + C_n(g) = Y_x@C_n(g). \tag{1}$$
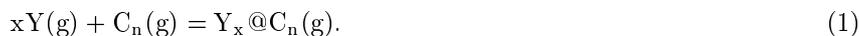
Table 1. Computed encapsulation potential-energy changes $\Delta E_{Y_x@C_n}$ (kcal/mol) for Li$_x$@C$_{60}$

Species	$\Delta E_{Y_x@C_n}$	$\frac{\Delta E_{Y_x@C_n}}{x}$ [a]
B3LYP[b]		
Li@C$_{60}$	-28.4	-28.4
Li$_2$@C$_{60}$	-51.1	-25.6
Li$_3$@C$_{60}$	-71.0	-23.7
MPWB1K[c]		
Li@C$_{60}$	-34.9	-34.9
Li$_2$@C$_{60}$	-62.8	-31.4
Li$_3$@C$_{60}$	-101.0	-33.7

[a] The relative term related to one Li atom. [b] Computed at the B3LYP/6-31G*//B3LYP/3-21G level. [c] Computed at the MPWB1K/6-31G*//MPWB1K/3-21G level.

The encapsulation process is thermodynamically characterized by the standard changes of, for example, enthalpy $\Delta H^o_{Y_x@C_n}$ or the Gibbs energy $\Delta G^o_{Y_x@C_n}$. In a first approximation, we can just consider the encapsulation potential-energy changes $\Delta E_{Y_x@C_n}$ (i.e., the differences in the total electronic energy between reactants and products). Table 1 presents the terms for Li$_x$@C$_{60}$. Their absolute values increase with the increasing number of the encapsulated Li atoms. In order to have some directly comparable relative terms, it is convenient to consider the reduced $\frac{\Delta E_{Y_x@C_n}}{x}$ terms related to one Li atom. Although the absolute values of the reduced term decrease with increasing Li content, the decrease is not particularly fast (so that, a further increase of the encapsulated Li atoms could still be possible). The MPWB1K terms are somewhat more pronounced and there is even a different trend for Li$_3$@C$_{60}$ compared to B3LYP (as shown by Zhao and Truhlar [30-35], B3LYP is however not particularly reliable for such situations). The computational findings help to rationalize why also the Li$_2$@C$_{60}$ species could be observed [11]. The basis set superposition error (BSSE) is not estimated for the presented values (a straightforward application of the Boys-Bernardi counterpoise method would be rather questionable in this situation, partly owing to a substantial cage deformation upon the encapsulation). However, the BSSE terms could be to some extent additive and thus, they should somewhat cancel out in a reaction series. Interestingly enough, the stabilization of metallofullerenes is mostly electrostatic as documented [45,46] using the topological concept of 'atoms in molecules' (AIM) [47,48] which shows that the metal-cage interactions form ionic (and not covalent) bonds.

The problem of the relative stabilities of clusters with different stoichiometries can also be considered in a series with variable metal, like Mg@C$_{74}$, Ca@C$_{74}$, Sr@C$_{74}$, and Ba@C$_{74}$. Let us consider an overall stoichiometry of a metallofullerene formation:

$$X(g) + C_n(g) = X@C_n(g). \tag{2}$$

The encapsulation process is thermodynamically characterized by the standard changes of, for example, enthalpy $\Delta H^o_{X@C_n}$ or the Gibbs energy $\Delta G^o_{X@C_n}$. The equilibrium composition of the reaction mixture is controlled by the encapsulation equilibrium constants $K_{X@C_n,p}$:

$$K_{X@C_n,p} = \frac{p_{X@C_n}}{p_X p_{C_n}}, \tag{3}$$

expressed in the terms of partial pressures of the components. The encapsulation equilibrium constant is interrelated with the the standard encapsulation Gibbs energy change:

$$\Delta G^o_{X@C_n} = -RTlnK_{X@C_n,p}. \tag{4}$$

Temperature dependency of the encapsulation equilibrium constant $K_{X@C_n,p}$ is then described by the van't Hoff equation:

$$\frac{dlnK_{X@C_n,p}}{dT} = \frac{\Delta H^o_{X@C_n}}{RT^2} \tag{5}$$

where the $\Delta H^o_{X@C_n}$ term is typically negative (as shown by available computations and also as expected in order to get a significant stabilization) so that the encapsulation equilibrium constants decrease with increasing temperature.

Let us further suppose that the metal pressure p_X is actually close to the respective saturated pressure $p_{X,sat}$. While the saturated pressures $p_{X,sat}$ for various metals are known from observations [49], the partial pressure of C$_n$ is

Table 2. The products of the encapsulation equilibrium constant[a] $K_{X@C_n,p}$ with the metal saturated-vapor pressure[b] $p_{X,sat}$ for Mg@C$_{74}$, Ca@C$_{74}$, Sr@C$_{74}$, and Ba@C$_{74}$ computed for illustrative temperatures $T = 1500$ and 2000 K

Endohedral	$K_{X@C_{74},p}$ (atm^{-1})	$p_{X,sat}$ (atm)	$p_{X,sat}K_{X@C_{74},p}$	$\frac{p_{X,sat}K_{X@C_{74},p}}{p_{Ba,sat}K_{Ba@C_{74},p}}$
		$T = 1500$ K		
Mg@C$_{74}$	5.78×10^{-8}	2.53	1.46×10^{-7}	4.2×10^{-9}
Ca@C$_{74}$	0.00919	0.162	0.00149	4.3×10^{-5}
Sr@C$_{74}$	0.518	0.355	0.184	5.3×10^{-3}
Ba@C$_{74}$	1332.6	0.0261	34.82	1.00
		$T = 2000$ K		
Mg@C$_{74}$	2.01×10^{-7}	16.6	3.34×10^{-6}	6.1×10^{-7}
Ca@C$_{74}$	0.00144	3.773	0.00542	9.9×10^{-4}
Sr@C$_{74}$	0.02694	6.124	0.1650	0.030
Ba@C$_{74}$	10.399	0.528	5.489	1.00

[a] The potential-energy change evaluated at the B3LYP/6-31G*~dz level and the entropy part at the B3LYP/3-21G~dz level; the standard state - ideal gas phase at 101325 Pa pressure.
[b] Extracted from available observed data [49].

less clear as it is obviously influenced by a larger set of processes (though, p_{C_n} should exhibit a temperature maximum and then vanish). However, at present there is no observed information available on the C$_n$ values. Therefore, we avoid the latter pressures in our considerations - in fact, they cancel out anyhow within a reaction series which is our case here. As already mentioned, the computed equilibrium constants $K_{X@C_n,p}$ have to show a temperature decrease with respect to the van't Hoff equation (5). However, if we consider the combined $p_{X,sat}K_{X@C_n,p}$ term:

$$p_{X@C_n} \sim p_{X,sat}K_{X@C_n,p}, \tag{6}$$

that directly controls the partial pressures of various X@C$_n$ encapsulates in an endohedral series (based on one common C$_n$ fullerene), we get a different picture. The considered $p_{X,sat}K_{X@C_n,p}$ term can frequently (though not necessarily) be increasing with temperature so that a temperature enhancement of metallofullerene formation in the electric-arc technique is still possible. An optimal production temperature could be evaluated in a more complex model that also includes temperature development of the empty-fullerene partial pressure.

If we however want to evaluate production abundances in a series of metallofullerenes like Mg@C$_{74}$, Ca@C$_{74}$, Sr@C$_{74}$ and Ba@C$_{74}$, just the product $p_{X,sat}K_{X@C_{74},p}$ terms can straightforwardly be used. The metal atoms are computed here in a dz basis set [50] with the effective core potential (ECP) so that the geometry optimizations are carried out at the B3LYP/3-21G~dz level and the energetics then evaluated at the B3LYP/6-31G*~dz level. It is a common practice to compute entropy at a lower level and the related energetics at a higher level of theory as entropy does not change considerably with a basis-set extension. The results in Table 2 show several interesting features. While for Mg@C$_{74}$ and Ca@C$_{74}$ the $p_{X,sat}K_{X@C_{74},p}$ quotient increases with temperature, it is about constant for Sr@C$_{74}$ for the considered temperatures, and it decreases with temperature for Ba@C$_{74}$. This behavior results from a competition between the decreasing encapsulation equilibrium constants and increasing saturated metal pressures. As the encapsulation enthalpy $\Delta H^o_{X@C_n}$ has the most negative value for Ba@C$_{74}$, its encapsulation equilibrium constant has to exhibit the fastest temperature decrease that already cannot be overcompensated by the temperature increase of the saturated metal pressure so that the $p_{X,sat}K_{X@C_{74},p}$ quotient decreases with temperature in this case. In order to allow for cancellation of various factors introduced by the computational approximations involved, it is better to deal with the relative quotient $\frac{p_{X,sat}K_{X@C_{74},p}}{p_{Ba,sat}K_{Ba@C_{74},p}}$. Table 2 shows that the production yield of Sr@C$_{74}$ should be by two or three orders of magnitude smaller than that for Ba@C$_{74}$. For Ca@C$_{74}$ the production yield for the considered temperatures is computed to be between three and five orders of magnitude lower than for Ba@C$_{74}$, and for Mg@C$_{74}$ between seven and nine orders. In principle, an endohedral with lower value of the encapsulation equilibrium constant can still be produced in larger yields if a convenient over-compensation by higher saturated metal pressure can take place.

Although the energy terms are likely still not precise enough, their errors are frequently comparable in reaction series. If this is also the case in our encapsulation series, the errors should cancel out in the relative term $\frac{p_{X,sat}K_{X@C_{74},p}}{p_{Ba,sat}K_{Ba@C_{74},p}}$. This should be the case of, for example, the basis set superposition error important for evaluation of the encapsulation potential-energy changes. A similar cancellation should also operate for the higher corrections to the rigid-rotor and harmonic-oscillator partition functions, including motions of the encapsulate. The motion of the endohedral atom is

highly anharmonic, however, its description is yet possible only with simple potential functions. Another option for evaluation of the entropic term could be classical molecular dynamics. As long as we are interested in the relative production yields, the anharmonic effects should at least to some extent be cancelled out in the relative quotient $\frac{p_{X,sat}K_{X@C_{74},p}}{p_{Ba,sat}K_{Ba@C_{74},p}}$. Incidentally, the computed stability proportions do correlate with qualitative abundances known from observations. For $Ba@C_{74}$ even microcrystals could be prepared [26] so that a diffraction study was possible, while for $Sr@C_{74}$ at least various spectra could be recorded [25] in solution, $Ca@C_{74}$ was studied [24] only by NMR spectroscopy, and $Mg@C_{74}$ is yet unknown from experiment.

ACKNOWLEDGMENTS

REFERENCES

[1] Haddon RC, Hebard AF, Rosseinsky MJ, Murphy DW, Duclos SJ, Lyons KB, Miller B, Rosamilia JM, Fleming RM, Kortan AR, Glarum SH, Makhija AV, Muller AJ, Eick RH, Zahurak SM, Tycko R, Dabbagh G, Thiel FA. Conducting films of C_{60} and C_{70} by alkali-metal doping. Nature 1991; 350: 320-2.
[2] Dunlap BI, Ballester JL, Schmidt, PP. Interactions between C_{60} and endohedral alkali atoms. J Phys Chem 1992; 96: 9781-7.
[3] Joslin CG, Yang J, Gray CG, Goldman S, Poll JD. Infrared rotation and vibration-rotation bands of endohedral fullerene complexes - absorption-spectrum of $Li^+@C_{60}$ in the range 1-1000 cm^{-1}. Chem Phys Lett 1993; 208: 86-92.
[4] Kaplan T, Rasolt M, Karimi M, Mostoller M. Numerical simulation of He^+ and Li^+ collisions with C_{60}. J Phys Chem 1993; 97: 6124-6.
[5] Wan ZM, Christian JF, Basir Y, Anderson SL. Collision of alkali ions with C_{60}/C_{70} - insertion, thermionic emission, and fragmentation. J Chem Phys 1993; 99: 5858-70.
[6] Joslin CG, Gray CG, Goldman S, Yang J, Poll JD. Raman spectra of endohedral fullerenes - $Li^+@C_{60}$. Chem Phys Lett 1993; 215: 144-50.
[7] Slanina Z, Adamowicz L. MNDO study of charged complexes of dodecahedron-shaped C_{20} with Li. J Mol Struct (Theochem) 1993; 281: 33-7.
[8] Varganov SA, Avramov PV, Ovchinnikov SG. Ab initio calculations of endo- and exohedral C_{60} fullerene complexes with Li^+ ion and the endohedral C_{60} fullerene complex with Li_2 dimer. Phys Solid Stat 2000; 42: 388-92.
[9] Slanina Z, Lee S-L. Quantum-chemical studies of superconducting fullerene derivatives. Chin J Phys 1996; 34: 633-7.
[10] Bol A, Stott MJ, Alonso JA. Density functional pseudopotential study of the endohedral complex $Li_2@C_{60}$. Physica B 1997; 240: 154-66.
[11] Kusch C, Krawez N, Tellgmann R, Winter B, Campbell EEB. Thermal desorption spectroscopy of fullerene films containing endohedral $Li@C_{60}$. Appl Phys A 1998; 66: 293-8.
[12] Slanina Z, Uhlík F, Lee S-L, Adamowicz L. Quantum-chemical calculations of model systems of interest in fullerene-based superconductivity. J Low Temp Phys 2003; 131: 1259-63.
[13] Gromov A, Lassesson A, Jönsson M. Ostrovskii DI, Campbell EEB. IR spectroscopy investigation of purified endohedral $Li@C_{60}$ and $Li@C_{70}$. In: Kamat P, Guldi D, Kadish K, Eds. Fullerenes: The exciting world of nanocages and nanotubes, PV 2002-12, The Electrochemical Society, Pennington, 2002; vol. 12: pp. 621-9.
[14] Gromov A, Krawez N, Lassesson A, Ostrovskii DI, Campbell EEB. Optical properties of endohedral $Li@C_{60}$. Curr App Phys 2002; 2: 51-5.
[15] Slanina Z, Uhlík F, Chow TJ. Non-central location of Li in $Li@C_{60}$. In: Guldi DM, Kamat PV, D'Souza F, Eds. Fullerenes and nanotubes: The building blocks of next generation nanodevices, PV 2003-15, The Electrochemical Society, Pennington, 2003; vol. 13: pp. 569-574.
[16] Campbell EEB. Fullerene Collision Reactions, Kluwer Academic Publishers: Dordrecht; 2003.
[17] Popok VN, Azarko II, Gromov AV, Jonsson M, Lassesson A, Campbell EEB. Conductance and EPR study of the endohedral fullerene $Li@C_{60}$. Sol Stat Commun 2005; 133: 499-503.
[18] Lassesson A, Hansen K, Jonsson M, Gromov A, Campbell EEB, Boyle M, Pop D, Schulz CP, Hertel IV, Taninaka A, Shinohara, H. A femtosecond laser study of the endohedral fullerenes $Li@C_{60}$ and $La@C_{82}$. Eur Phys J D 2005; 34: 205-9.
[19] Gurin VS. Endofullerenes with small silver and copper clusters. Int J Quantum Chem 2005; 104: 249-55.
[20] Gurin VS. Ab initio calculation of endohedal fullerenes with copper and silver clusters. Fullerene Nanotub Carb Nanostruct 2005; 13: Suppl. 1, 3-11.
[21] Slanina Z, Uhlík F, Lee S-L, Adamowicz L, Nagase S. Computations of endohedral fullerenes: The Gibbs energy treatment. J Comput Meth Sci Engn 2006; 6: 243-50.
[22] Pavanello M, Jalbout AF, Trzaskowski B, Adamowicz L. Fullerene as an electron buffer: Charge transfer in $Li@C_{60}$. Chem Phys Lett 2007; 442: 339-43.
[23] Wan TSM, Zhang HW, Nakane T, Xu ZD, Inakuma M, Shinohara H, Kobayashi K, Nagase S. Production,

isolation, and electronic properties of missing fullerenes: $Ca@C_{72}$ and $Ca@C_{74}$. J Am Chem Soc 1998; 120: 6806-7.

[24] Kodama T, Fujii R, Miyake Y, Suzuki S, Nishikawa H, Ikemoto I, Kikuchi K, Achiba Y. ^{13}C NMR study of $Ca@C_{74}$: The cage structure and the site-hopping motion of a Ca atom inside the cage. Chem Phys Lett 2004; 399: 94-7.

[25] Haufe O, Hecht M, Grupp A, Mehring M, Jansen M. Isolation and spectroscopic characterization of new endohedral fullerenes in the size gap of C_{74} to C_{76}. Z Anorg Allgem Chem 2005; 631: 126-30.

[26] Reich A, Panthofer M, Modrow H, Wedig U, Jansen M. The structure of $Ba@C_{74}$. J Am Chem Soc 2004; 126: 14428-34.

[27] Becke AD. Density-functional thermochemistry. III. The role of exact exchange. J Chem Phys 1993; 98: 5648-52.

[28] Lee C, Yang W, Parr RG. Development of the Colle-Salvetti correlation-energy formula into a functional of the electron density. Phys Rev B 1988; 37: 785-9.

[29] Frisch MJ, Trucks GW, Schlegel HB, Scuseria GE, Robb MA, Cheeseman JR, Montgomery Jr. JA, Vreven T, Kudin KN, Burant JC, Millam JM, Iyengar SS, Tomasi J, Barone V, Mennucci B, Cossi M, Scalmani G, Rega N, Petersson GA, Nakatsuji H, Hada M, Ehara M, Toyota K, Fukuda R, Hasegawa J, Ishida M, Nakajima T, Honda Y, Kitao O, Nakai H, Klene M, Li X, Knox JE, Hratchian HP, Cross JB, Adamo C, Jaramillo J, Gomperts R, Stratmann RE, Yazyev O., Austin AJ, Cammi R, Pomelli C, Ochterski JW, Ayala PY, Morokuma K, Voth GA, Salvador P, Dannenberg JJ, Zakrzewski VG, Dapprich S, Daniels AD, Strain MC, Farkas O, Malick DK, Rabuck AD, Raghavachari K, Foresman JB, Ortiz JV, Cui Q, Baboul AG, Clifford S, Cioslowski J, Stefanov BB, Liu G, Liashenko A, Piskorz P, Komaromi I, Martin RL, Fox DJ, Keith T, Al-Laham MA, Peng CY, Nanayakkara A, Challacombe M, Gill PMW, Johnson B, Chen W, Wong MW, Gonzalez C, Pople JA. Gaussian 03, Revision C.01, Gaussian, Inc.: Wallingford, CT; 2004.

[30] Zhao Y, Truhlar DG. Hybrid meta density functional theory methods for thermochemistry, thermochemical kinetics, and noncovalent interactions: The MPW1B95 and MPWB1K models and comparative assessments for hydrogen Bonding and van der Waals interactions. J Phys Chem A 2004; 108: 6908-18.

[31] Zhao Y, Lynch BJ, Truhlar DG. Multi-coefficient extrapolated density functional theory for thermochemistry and thermochemical kinetics. ChemPhysChem 2005; 7: 43-52.

[32] Zhao Y, Truhlar DG. Multi-coefficient extrapolated DFT studies of pi...pi interactions: The benzene dimer. J Phys Chem A 2005; 109: 4209-12.

[33] Zhao Y, Truhlar DG. How well can new-generation density functional methods describe stacking interactions in biological systems? Phys. Chem Chem Phys 2005; 7: 2701-5.

[34] Zhao Y, Truhlar DG. The design of density functionals that are broadly accurate for thermochemistry, thermo-chemical kinetics, and nonbonded interactions. J Phys Chem A 2005; 109: 5656-67.

[35] Zhao Y, Truhlar DG. Benchmark databases for nonbonded interactions and their use to test density functional theory. J Chem Theory Comput 2005; 1: 415-32.

[36] Perdew JP, Wang Y. Accurate and simple analytic representation of the electron-gas correlation energy. Phys Rev B 1992; 45: 13244-9.

[37] Becke AD. Density-functional thermochemistry. IV. A new dynamical correlation functional and implications for exact-exchange mixing. J Chem Phys 1996; 104: 1040-6.

[38] Hehre WJ, Radom L, Schleyer PvR, Pople, JA. Ab Initio Molecular Orbital Theory, J. Wiley Inc.: New York; 1986.

[39] Logan RA, Cote RE, Kusch P. The sign of the quadrupole interaction energy in diatomic molecules. Phys Rev 1952; 86: 280-7.

[40] Brooks RA, Anderson CH, Ramsey NF. Rotational magnetic moments of diatomic alkalis. Phys Rev Lett 1963; 10: 441-3.

[41] Huber KP, Herzberg G. Molecular Spectra and Molecular Structure, IV. Constants of Diatomic Molecules, Van Nostrand Reinhold Company: New York; 1979.

[42] Blanc J, Broyer M, Chevaleyre J, Dugourd P, Kuhling H, Labastie P, Ulbricht M, Wolf JP, Wöste L. High resolution spectroscopy of small metal clusters. Z Phys D 1991; 19: 7-12.

[43] Kawai R, Tombrello JF, Weare JH. Li_5 as a pseudorotating planar cluster. Phys Rev A 1994; 49: 4236-9.

[44] Slanina Z, Rudziński JM, Togasi M, Ōsawa E. Quantum-chemically supported vibrational analysis of giant molecules: The C_{60} and C_{70} clusters. J Mol Struct (Theochem) 1989; 202: 169-76.

[45] Nagase S, Kobayashi K, Akasaka T. Recent progress in endohedral dimetallofullerenes. J Mol Struct (Theochem) 1997; 398/399: 221-7.

[46] Kobayashi K, Nagase S. Bonding features in endohedral metallofullerenes. Topological analysis of the electron density distribution. Chem Phys Lett 1999; 302: 312-6.

[47] Bader RFW. A quantum theory of molecular structure and its applications. Chem Rev 1991; 91: 893-928.

[48] Bader RFW. A bond path: A universal indicator of bonded interactions. J Phys Chem A 1998; 102: 7314-23.

[49] Alcock CB, Itkin VP, Horrigan MK. Vapor pressure equations for the metallic elements: 298-2500 K. Can Metallurg Quart 1984; 23: 309-13.

[50] Hay PJ, Wadt WR. Ab initio effective core potentials for molecular calculations. Potentials for K to Au including the outermost core orbitals. J Chem Phys 1985; 82: 299-310.